In **Remote Sensing of the Changing Oceans**
Tang, DanLing (Ed.)
1st Edition., May 2011, VIII, 449 p. 182 illus., 130 in color., Hardcover
ISBN: 978-3-642-16540-5

The original publication is available at http://www.springer.com/

Satellite Air – Sea Fluxes

A. Bentamy[1, *] , K .Katsaros[2], and P. Queffeulou[1]

[1] Institut Français pour la Recherche et l'Exploitation de la MER (IFREMER), Plouzané, France
[2] Rosenstiel School of Marine and Atmospheric Sciences, University of Miami, Miami, Florida and Northwest Research Associates, Bellevue, Washington, USA

*: Corresponding author : A. Bentamy, email address : Abderrahim.Bentamy@ifremer.fr

Abstract:

This chapter addresses the estimation of global surface winds, surface wind stress, latent heat flux, and sensible heat flux over the oceans with high spatial and temporal resolution using satellite radar and radiometer measurements. An overview of the physics of remotely sensed data, of methods and algorithms used to retrieve surface fluxes is provided. The retrievals are used to estimate regular in space and time surface parameters, requested for oceanic forcing function, over global ocean. The characteristics of the former are investigated at global and regional scales.

1. Introduction

The large exchanges of energy between ocean and atmosphere through air-sea fluxes at the interface, the absorption of radiation from the sun in the upper ocean, and the redistribution of heat by the ocean circulation at all time and space scales, characterize the main role of the ocean in climate variability. Surface fluxes of momentum, heat, and water vapor provide some of the dominant processes that are involved. For several reasons and especially at large scales, the measurement of the relevant oceanic surface properties is quite difficult. It is common to use parameterization methods to estimate surface fluxes based on the knowledge of some basic variables such as surface wind, sea surface temperature, air temperature, and surface and air humidity. The latter can be estimated from buoy, ship, and satellite data. We usually rely on the bulk aerodynamic formulae that parameterize the fluxes in terms of the observed mean quantities. The surface fluxes derived from satellite observations are expressed as follows:

$$^{\tau} = (^{\tau}x\ ,^{\tau}y\ ) = \rho\ C\ U(u,v)$$

$$^{Q}latent = -l\rho\ CE\ U\ (qa - qs)$$

$$Q_{sens} = -\rho C_p C_T \overline{U}(T_a - T_s) \quad (3)$$

where τ is the vector wind stress with zonal τ_x *and* meridional τ_y wind stress components; Q_{latent} and Q_{sens} are the latent and sensible heat fluxes; $\overline{U}$ is the magnitude of the surface wind vector (wind speed) at 10 m height under neutral stratification which has zonal u and meridional v vector wind components; q_a and q_s are the air and surface (or saturation) specific humidity; T_a is the dry bulb temperature; T_s is the sea surface temperature; l is the coefficient for latent heat of evaporation considered as constant 2.5×10^6 J kg^{-1}; ρ is the air density at observation level, calculated from mean surface temperature and sea-level pressure using the ideal gas equation with a correction for the virtual temperature to compensate for the behavior of moist air; C_P the specific heat at constant pressure is approximated to be constant 1.0×10^3 J kg^{-1} K^{-1}. C_D and C_E, and C_T are the bulk drag coefficient, the transfer coefficient for water vapor, and the transfer coefficient for sensible heat, respectively.

Since our estimates of the surface fluxes are based on the bulk approach, their quality would be related to the accuracy of surface wind, air and sea temperature, and of air and near surface humidity. This paper describes the methods and the algorithms used to retrieve these parameters from radar and radiometer measurements onboard polar orbiting satellites.

2. REMOTELY SENSED DATA

2.1. Scatterometer

2.1.1. General topics

Since 1991 five scatterometers have been launched onboard polar-orbiting satellites: European Remote Sensing Satellites 1 and 2 (ERS-1/2), Advanced Earth Observing Satellites 1 and 2 (ADEOS-1/2), QuikScat and METOP. The scatterometer is an active radar sending microwave pulses to the ocean surface and measuring the power backscattered from surface roughness. The backscatter is mainly related to the small centimeter waves on the surface. Indeed, it was established that the ocean surface ripples are in equilibrium with local wind stress. Jones *et al.*(1978) showed, based on measurements from aircraft experiments that for incidence angle greater than 20°, the backscatter coefficient increases with respect to wind speed. They also demonstrated the anisotropic characteristics of the scattering. It was established that the backscatter coefficient σ^0 is not only a function of wind speed, but also of wind direction relative to the radar azimuth. The scatterometer is the unique radar providing wind speed as well as wind direction over the global ocean.

The study of the relationship between σ^0 measurements and the surface wind vector is still ongoing: indeed, many current works aim to establish a physical backscatter model. However, the theory relating wind speed to wave generation and equilibrium spectrums is not well developed. Therefore, only empirical models are currently determined and used to establish a relation between the backscatter coefficient and wind speed and direction for some specific incidence angles, radar azimuth, and polarization.

The European Space Agency launched two scatterometers using identical instruments onboard ERS-1 (August 1991) and ERS-2 (April 1995). Both are composed of three antennas (fore-, mid-, and aft-beam) operating at C-band (5.33 GHz) with only vertical polarization (VV). ERS scatterometers scan a 500 km swath on one side of the satellite, and measure at three azimuth angles: 45°, 90°, and 115°. The incidence angle varies from 17° to 46° for the mid beam and from 25° to 57° for fore- and aft-beams (Figure 1). The scatterometer swath is divided into cells of 50km×50km separated by 25km distance. Hereafter, the scatterometer cell over the ocean is referred to as a wind vector cell (WVC). Over each WVC, a backscatter coefficient might be provided by each antenna. They are used to calculate speed and direction through inverse and direct models. Two kinds of ERS scatterometer winds are available. Near real time data processed by ESA, and off line processed, archived, and distributed by the Centre ERS d'Archivage et de Traitement (CERSAT/IFREMER). The latter are called WNF (WiNd Field). The calibration and validation of the algorithms were performed with dedicated buoy data during the RENE91 experiment, with the National Oceanic and Atmospheric Administration (NOAA) National Data Buoy Center (NDBC) buoys and the Tropical Ocean Global Atmosphere (TOGA) Tropical Atmosphere Ocean (TAO) buoys. The accuracy of the wind speed and direction derived from the IFREMER algorithm is about 1m/s and 14°. The validation of the off-line wind products indicated that, at low wind speeds, data are less accurate in wind speed and direction determination (Graber *et al.*, 1996).

In August 1996, the National Aeronautics and Space Administration (NASA) launched the scatterometer called NSCAT on board Japanese satellite ADEOS-1 (or Midori). It is in a circular orbit with a period of 101 minutes at an inclination of 98.59° and at a nominal height of 796 km with a 41-day repeat cycle. NSCAT had two 600 km wide swaths located on each side of the satellite track and separated by 300 km (Figure 1). It operated at 14 GHz (Ku band). Its fore-beam and aft-beam antennas pointed at 45° and 135° to each side of the satellite track, respectively. The mid-beam pointed at 65° and 115° depending on the NSCAT swath. The fore and aft-beams provide σ^0 measurements with vertical polarization and incidence angle varying between 19° and 63°. The mid-beam provided two σ^0 measurements corresponding to vertical and horizontal polarizations with an incidence angle varying between 16° and 52°. The spatial resolution of the instrument on the earth's surface was about 25km.

Following theADEOS-1 breakdown, NASA launched the SeaWinds scatterometer onboard the QuikSCAT satellite on 19th July 1999. This satellite operated for 10 full years. QuikScat/SeaWinds had a rotating antenna with two differently polarized emitters: the H-pol with incidence angle of 46.25° and V-pol with incidence angle of 54° (Figure 1). The inner beam had a swath of about 1400km, while the outer beam swath was 1800km width. The spatial resolution of SeaWinds (oval footprint) was 25×35 km. The latter were binned over the scatterometer swath into WVC of 25×25 km. There are 76 WVC across the satellite swath, and each contains the center of 10 to 25 measured σ^0. The remotely sensed wind vectors are estimated from the scatterometer σ^0 over each WVC using the empirical model QSCAT-1 relating the measured backscatter coefficients to surface winds. The standard SeaWinds wind retrievals are referenced as L2B products. They have been calculated using the standard scatterometer method based on the Maximum Likelihood Estimator (MLE) (JPL, 2001**)**. The scatterometer retrieval algorithm estimates several wind solutions for each wind cell. In general, there are four solutions. The ambiguity removal method is then used to select the most probable wind solution. The latter are used in this study. To improve the wind direction, especially in the middle of a swath, where the azimuth diversity is quite poor, an algorithm called Direction Interval Retrieval with Threshold Nudging (DIRTH) is used too. SeaWinds is a Ku band radar. Therefore, rain has a substantial influence on its measurements. Previous studies (Sobieski *et al.*, 1999) showed that the rain impact may attenuate the scatterometer signal, resulting in wind speed underestimation, or change the surface shape due to raindrop impact and splatter, leading to an overestimation of the retrieved winds. The SeaWinds wind products involve several rain flags determined from the scatterometer observations and from the collocated radiometer rain rate onboard other satellites.

An identical SeaWinds scatterometer was launched by NASA onboard the second Japanese satellite, ADEOS-2, in December 2002. It operated until June 2003. The QuikScat/SeaWinds surface wind estimations will be indicated by QuikScat hereafter.

The latest remotely sensed surface wind-measuring instrument is the Advanced SCATterometer (ASCAT). It was launched aboard the European Meteorological Satellite Organization (EUMESAT), MetOp-A on October 19, 2006. Scientific and technical documentation related to ASCAT physical measurements as well as to ASCAT derived products may be found at the EUMETSAT web site http://www.eumetsat.int/Home/Main/Publications/Technical_and_Scientific_Documentation/Technical_Notes/ and under EUMETSAT Ocean & Sea Ice Satellite Application (O&SI SAF) web site (http://www.osi-saf.org/) . MetOp is in a circular orbit (near synchronous orbit) for a period of about 101 minutes, at an inclination of 98.59° and at a nominal height of 800 km with a 29-day repeat cycle. ASCAT has two swaths 550 km wide, located on each side of the satellite track, separated by 700km. It operates at 5.3 GHz (C band). Its fore-beam and aft-beam antennas point at 45° and 135° on each side of the satellite track, respectively. The mid-beam antennas point at 90°. The ASCAT beams measure normalized radar cross sections with vertical polarization, σ^0, which are a dimensionless property of the surface, describing the ratio of the effective echoing area per unit area illuminated. The fore and aft-beams provide backscatter coefficient measurements at incidence angle varying between 34° and 64°. The mid-beams provide σ^0 measurements at incidence angle varying between 25° and 53°. Two Backscatter coefficient spatial resolutions are available over global ocean: 25km and 12.5km.

2.1.2. Scatterometer wind retrievals

Retrieving wind velocity from sea state is a not trivial inverse problem. Indeed, results obtained via boundary-layer theories give relations to link a given wind vector over the sea surface to momentum exchange between air and sea. This momentum is then related to sea roughness properties (wave height, slope, etc.). Nevertheless, the inverse problem (from a value of sea roughness to an associated wind vector) is not yet fully based on theory. Another attempt deals with global ocean wind sea retrieval. Indeed, the actual knowledge of the atmospheric boundary layer is more concerned with a sea at an equilibrium state than for specific regions (closed seas with limited fetch). The model function which relates a wind vector to a sea state has then to be a Global Model Function (GMF).

The general GMF form used for scatterometers is based on a truncation of the Fourier expansion of σ^0 over the azimuth angle range:

$$\sigma^0 (U, \varphi, \theta, P) = A0(U,\theta,P) + A1(U,\theta,P)\times\cos(\varphi) + A2(U,\theta,P)\times\cos(2\varphi) \qquad (4)$$

Where φ is the difference between the wind direction and measurement azimuth, U the wind speed, θ the incidence angle, and P the polarization.

The GMF and the inverse algorithm are supposed to be valid for the global oceans. Therefore some local events (in space and time) that might modify the ripple wave spectrum and then degrade the scatterometer retrieved wind vectors are not explicitly taken into account. Examples of such effects include: the interaction of short waves with longer ocean surface waves, the damping of waves trough natural or artificial surface slicks, the impact of the atmospheric boundary layer stability on the generation of ripple waves, and other local sea state characteristics. The impact of such perturbations might be detected through quality control procedures.

The determination of GMF model coefficients *A0*, *A1*, and *A2* is performed using a control optimal method minimizing the difference between measured and simulated (from GMF) backscatter coefficients. The latter are estimated from collocated buoy and/or numerical weather prediction (NWP) wind speed and direction. Figure 2 shows an example of behavior of measured (dots) and simulated (line) σ^0 as a function of wind direction for three wind speed and incidence angle ranges. The maximum σ^0 values are reached for relative wind direction of 0° (upwind) and 180° (downwind). The minimums are located at 90° and 270° (crosswind).

The determination of surface wind speed and direction from the knowledge of measured backscatter coefficients over a given WVC, requires some assumptions. First we assume that measured σ^0 are expressed as

$$\sigma^0 = \sigma^0_P + \varepsilon \qquad (5)$$

where σ^0_P represents « truth » for the backscatter coefficient and ε is the error related to instrument and physics of the measurement, surface conditions, and to the calibration and validation procedures. ε is assumed Gaussian with zero mean and variance δ_ε.

It is also assumed that σ^0_P is related to GMF through :

$$\sigma^0_{\boldsymbol{P}} = \sigma^0_{\boldsymbol{mod}} + \varepsilon_{\boldsymbol{mod}} \qquad (6)$$

σ^0_{mod} is backscatter coefficient value estimated from (4), and $\varepsilon_{\boldsymbol{mod}}$ is the model error assumed Gaussian with $\delta\varepsilon_{mod}$ variance.

For a given wind speed and direction over WVC, the difference between measured and simulated backscatter coefficients is calculated:

$$\Delta = \sigma^0 - \sigma^0_{\boldsymbol{mod}} \qquad (7)$$

Assuming that instrumental and model errors are independent, Δ is gaussian with zero mean and variance $\delta_\Delta = \delta_\varepsilon + \delta_{\varepsilon mod}$

Therefore the probability density function of Δ constrained by σ^0 becomes:

$$P(\Delta/\sigma^0) = P(\Delta/\{U,\varphi\}) = \frac{1}{\sqrt{2\pi\delta_\Delta}} exp\left(-\frac{\Delta^2}{2\delta_\Delta}\right) \qquad (8)$$

Let us consider N to be the number of σ^{0}'s over WVC (3 in the case of ERS), and that the corresponding Δ 's are independent. The conditional probability is then provided by:

$$P\,(\Delta_1 \ldots \Delta_N / \{U,\varphi\}) = \prod_{i=1}^{N} \frac{1}{\sqrt{2\pi\delta\Delta_i}} exp(-\sum_{i=1}^{N} \frac{\Delta_i^2}{2\delta\Delta_i}) \qquad (9)$$

The maximum likelihood estimator (MLE) criterion implies that the solution $\{U, \varphi\}$ is the local minimum of *P*. In general, over each WVC the wind speed and direction solutions are determined as a maximum of the following function:

$$J\,(U,\varphi) = \sum_{i=1}^{N} \frac{(\sigma_i^0 - \sigma_{i\,mod}^0(U,\varphi))^2}{\delta\Delta_i} + ln(\delta\,\Delta_i) \qquad (10)$$

J is related to *P* through a logarithmic transform.

The algorithm proposes up four solutions, called ambiguities. The most probable vector is indicated as the selected wind vector for the specific WVC. This selection is mainly based on the MLE and quality control (QC) use (See for instance Quilfen, 1995 ; Stoffelen *et al.*, 1997 , Freilich et al, 1999, Thiria *et al.*, 1993). Examples of selected wind speed and direction derived from QuikScat measurements are shown in Figure 3. Each panel presents wind speed and direction estimated over WVC of an available QuikScat swath crossing the Mediterranean Sea.

2.1.3. Scatterometer wind accuracy

The accuracies of scatterometer retrieval wind speed and direction are commonly determined through comparisons with buoy wind measurements. Four buoy networks are used to estimate the quality of the retrieved scatterometer wind vectors: the National Data Buoy Center (NDBC) buoys-off the U.S. Atlantic, Pacific and Gulf coasts maintained by the National Oceanic and Atmospheric Administration (NOAA); the Tropical Atmosphere Ocean (TAO) buoys located in tropical Pacific Ocean and maintained by the NOAA Pacific Marine Environmental Laboratory (PMEL); the European buoys-off European coasts called ODAS and maintained by U.K. Met office and Meteo-France; and the Pilot Research Moored Array in the Tropical Atlantic (PIRATA) moored in the Tropical Atlantic ocean and maintained by the Institut pour la Recherche et le Développement (IRD), the Instituto Nacional de Pesquisas Espaciais (INPE), and PMEL.

2.1.3.1. Collocated buoy and scatterometer data

For each buoy network and scatterometer (ERS-1/2, NSCAT, and QuikScat), the spatial collocation between anemometer and remotely sensed data is achieved by selecting satellite WVCs which fall within a 2°×2° square centered around the buoy location (Longitude and latitude). Temporal collocation is performed by choosing the buoy observation closest to the time of satellite overpass. In general the buoy observations are hourly reported. Hourly PIRATA data are calculated from 10-minute observations. Only available and validated (based on quality control procedures) buoy and scatterometer data are used in the comparisons. Furthermore, for accuracy purposes, only buoys located in deep water and far enough from coast are considered because no shallow water effects are taken into account. The calculation of buoy wind speed at 10m height in neutral conditions is performed using boundary layer model (Liu *et al.*, 1979). For the four networks, only hourly buoy wind speed and direction estimates are used in the scatterometer/buoy wind comparisons.

2.1.3.2. Statistical parameters

Comparison procedures are based on the following statistical parameters:

$$\overline{X} = E(X) \tag{11}$$

$$\sigma_X = \sqrt{E(X - E(X))^2} \tag{12}$$

$$\gamma_X = \frac{E(X - E(X))^3}{(E(X - E(X))^2)^{3/2}} \tag{13}$$

$$K_X = \frac{E(X - E(X))^4}{(E(X - E(X))^2)^2} \tag{14}$$

X stands for wind speed (or wind component) variable

E stands for the first conventional moment.

The surface wind variable is often considered as stochastic. Therefore, it may be described using linear moments in addition to using conventional moments; the advantage of using linear moments is their small sensitivity to erroneous measurements and/or estimates that yields outliers in data (Hosking, 1990).

The n^{th} linear moment is defined as

$$\lambda_n=\int_0^1 x(F)P^*_{n-1}(F)dF \qquad (15)$$

F is the probability function of *X*, *x(F)* is the inverse function of *F*, called quantile function, P^*_n are orthogonal polynomial functions related to the Legendre polynomials **through** $P^*_n=P_n(2s-1)$ **,** $s\in]0,1[$ **.**

Finally, the comparisons are also characterized by the linear regression coefficients; Let X and Y be two wind variables (model and satellite), the linear dependence between them is described as:

$$\tilde{Y}=aX+b \qquad (16)$$

$a=\frac{Syx}{Sxx}$ and $b = E(Y) - aE(X)$

$Syx = E(Y-E(Y))E(X-E(Y))$ and $Sxx = E(X-E(X))^2$

As the error characteristics of the model and the scatterometer are not known, it is more efficient to estimate the symmetrical regression coefficients: $\tilde{Y}_s=a_s X+b_s$

$$a_s=\sqrt{\frac{Syy}{Sxx}} \qquad (17)$$

the correlation coefficient is defined as

$$\rho = \frac{Syx}{\sqrt{SxxSyy}} \quad . \qquad (18)$$

For wind direction, the parameters mean difference (9), standard deviation of the difference (10), and vector correlation (11) are used. They take into account the circular behaviour of such variables.

$$\overline{D}=tan^{-1}\left(\frac{<sin(Db-Ds)>}{<cos(Db-Ds)>}\right) \qquad (19)$$

Db and ***Ds*** are the collocated model and satellite wind directions, respectively.

$$\sigma_D=sin^{-1}(\varepsilon)(1+0.1547\varepsilon^3) \qquad (20)$$

From Yamartino (1984) $\varepsilon=\sqrt{1-((sin(\delta D))^2+(cos(\delta D))^2)}$

Where $sin\delta D=<sin(Db-Ds)>$ and $cos(\delta D)=<cos(Db-Ds)>$

$$\rho^2 = Tr((\Sigma_{11})^{-1}\Sigma_{12}(\Sigma_{22})^{-1}\Sigma_{21}) \quad (21)$$

Σ_{ij} is the cross-covariance matrix of the wind vector and *Tr* states for matrix track.

2.1.3.3. Results

Figures 4 and 5 show scatterometer wind speed and direction accuracy results, respectively. They show scatter plots of the comparisons of ERS-1, ERS-2, and QuikScat scatterometer wind speeds and directions with 10-m neutral winds derived from buoys moored in Atlantic (including NDBC and ODAS), : Pacific (NDBC), and in Tropical (including TAO and PIRATA) zones. The remotely sensed and buoy winds compare well. In general, correlation coefficients exceed 0.8 and rms differences are lower than 2m/s for wind speed and 25° for wind direction. The main discrepancies are found for low wind speed conditions. Excluding buoy winds less than 5m/s, the rms values drop to 1.2 m/s for wind speed and 18° for wind direction. However, the mean differences indicate a slight underestimation of ERS, and an overestimation of QuikScat wind speeds with respect to buoy measurements. Indeed, the bias values are about 0.4m/s, 0.7m/s, and –0.4m/s for ERS-1, ERS-2, and QuikScat, respectively. Using a large database involving a collocated buoy and satellite data set, empirical models are under development to reduce the remotely sensed wind biases.

2.2. Special Sensor Microwave Imager (SSM/I)

Since 1990 the SSM/I radiometers onboard the DMSP F10, F11, F13, , F14, and F15 satellites provide measurements of the surface brightness temperatures at frequencies of 19.35, 22.235, 37, and 85 GHz (hereafter referred to as 19, 22, 37, and 85 GHz), respectively. Horizontal and vertical polarization measurements are taken at 19, 37, and 85 GHz. Only vertical polarization is available from 22 GHz. Due to the choice of the channels operating at frequencies outside strong absorption lines [for water vapor] (50-70 GHz), the radiation observed by the antennae is a mixture of radiation emitted by clouds, water vapor in the air and the sea surface, as well as radiation emitted by the atmosphere and reflected at the sea surface. For estimation of the 10-m wind speed from SSM/I brightness temperatures, we used an algorithm published by Bentamy *et al..*. (1999). This algorithm is a slightly modified version of that published by Goodberlet *et al..*. (1989) that includes a water vapor content correction. The SSM/I wind speeds are calculated over swaths of 1394-km width, with a spatial resolution of 25 km ×25 km. Previous studies investigated the accuracies of the retrieved SSM/I winds through a comparison with wind speed and direction measured by moored buoys in several oceanic regions (Bentamy *et al.*. 2002). The retrieved wind speed was calculated from brightness temperature measurements provided by NASA Marshall Space Flight Center (MSFC). The standard error values of SSM/I wind speeds with respect to the buoy winds are less than 2 m/s. The bias values do not exceed 0.2 m/s.

The SSM/I measurements are also commonly used to estimate rain rate, latent and sensible heat fluxes. Several methods for estimating such parameters have been discussed in the literature (see for instance Liu, 1986; Miller and Katsaros, 1992; Schulz *et al.*, 1993; Schlüssel *et al.*, 1995; Bentamy *et al.*, 2003). The calculation of latent and sensible heat fluxes from satellite measurements is mainly based on the use of bulk formulae (Eqs. 2 and 3). It requires the knowledge of surface wind speed, the specific air and surface humidity, and the sea surface and air temperatures.

2.2.1. Specific air humidity

Several authors have investigated the estimation of specific air humidity (q_a) from microwave radiometer measurements. Liu (1986), used 17 yrs of soundings from ship and ocean-island stations to show that q_a (not necessarily at a 10-m height) is well correlated with the integrated water vapor content, W, which can be derived from SSM/I brightness temperatures. This method provides accurate values of global monthly-averaged q_a but exhibits a systematic bias grater than 2 g kg^{-2} in the Tropics, as well as in the mid and high latitudes. To reduce this bias, Miller and Katsaros (1992) derived regressions of the air-sea humidity difference as a function of W. Their model improves the estimation of instantaneous values but it is limited to the northwest Atlantic. Schulz et al. (1993) provided a model to estimate the SSM/I precipitable water of the lowest 500-m layer of the planetary boundary layer (bottom-layer-integrated water vapor W_B instead of W). The calibration of the SSM/I W_B is based on 542 globally distributed soundings derived from meteorological field experiments. In addition, they derived a linear relationship between W_B and q_a. Ataktürk and Katsaros (1998) applied the Schulz et al. (1993) model to individual estimations and found that it overestimated q_a values in the subtropics. Schlüssel et al. (1995), using a larger dataset of soundings, determined a new version of the Schulz model. In this model, q_a is derived directly from SSM/I brightness temperature measurements.

Several of the inverse models relating the specific humidity of air and SSM/I brightness temperature measurements were investigated through comparison with observations of q_a from ships. The model described by Schulz et al. (1993, 1997) provides better agreement with in situ q_a estimates than previous models**.** However, comparisons performed by Bentamy *et al.*, (2003) showed seasonal and regional biases between ship and satellite q_a calculated using the Schulz model. In the North Atlantic, this bias was about -0.22 g kg^{-1} during the summer season, while in the winter and spring seasons it was about 0.7-0.8 g kg^{-1}. Comparisons between ship and ODAS buoy q_a estimates did not show such biases. Therefore, to minimize these biases between satellite and in situ air specific humidity, a sample of 1000 pairs of collocated SSM/I brightness temperatures and ship data was used to estimate new values for the coefficients in the Schulz model. The collocation is performed over the global oceans, using all available and validated satellite (F10, F11, F13, and F14) and ship data during the period October 1996-September 1997. The collocated ship q_a data are divided into bins of 0.5 g kg^{-1}. From each q_a class, 20 of the collocated ship/satellite data were randomly selected. The q_a model coefficients were determined by minimizing the squared differences between observed q_a (from ship) and estimated q_a (from satellite). The new model and its coefficients are provided by the following equation:

$$q_a = a_0 + a_1T_{19V} + a_2T_{19H} + a_3T_{22V} + a_4T_{37V}, \tag{22}$$

where a_0 = -55.9227, a_1 = 0.4035, a_2 = -0.2944, a_3 = 0.3511, and a_4 = -0.2395.

The remaining collocated ship/satellite data are used to compare in situ and remotely sensed q_a estimates. As expected, the comparisons of the statistical parameters are improved using the new q_a model. On average, the bias is reduced by 15% and is no longer statistically significant. The rms difference between satellite and ship q_a estimates is now 1.40 instead of 1.70 g kg^{-1}. Over the North Atlantic Ocean (80% of ship data are located in this region), the maximum values of the difference bias between satellite and ship q_a is about 0.25 g kg^{-1} and is found during the summer season, where q_a values are high.

2.2.2. Latent heat flux

The remotely sensed surface wind speed and specific air humidity, described above, are used to estimate latent heat flux. The calculation of Q_{latent} is performed hourly, with a spatial resolution of 1° in latitude and 1° in longitude. This resolution is consistent with that of the Reynolds daily gridded maps used for SST retrieval. Prior to calculating Q_{latent}, all available data (winds, SSTs, and brightness temperatures), sampled within a 1° × 1° grid point of a satellite swath during a given hour, are averaged, and the two first statistical moments are computed.

Over each grid point located within each SSM/I swath, the available U_{10}, T_s, T_{19V}, T_{19H}, T_{22V}, and T_{37V} are used to estimate the instantaneous latent heat flux values through Eq. (2). In cases when the SSM/I wind speeds are not valid, scatterometer winds calculated over the same grid point and within a 3-h window are temporally interpolated to the time of the SSM/I observations. On average, the percentage of individual latent heat fluxes estimated with scatterometer wind speeds is about 15% for NSCAT and 9% for ERS-2. This number increases in tropical areas (10°S-10°N) to 19% for NSCAT and to 12% for ERS-2.

Several assumptions have been made for the calculations described above. The SST at a grid point is assumed constant over a day. The surface pressure P_0 is assumed to be at a constant value of 1013.25 hPa. Air temperature at 10 m, T_{10}, is taken to be T_s–1.25 K. The impact of these assumptions on bulk latent heat flux estimation has been investigated with buoy measurements, which provide surface pressure, air temperature, and sea surface temperatures. The possible error (uncertainty) due to these assumptions is generally less than 2.5%.

2.3. Altimeter

Satellite altimeters routinely provide along-track measurements of surface wind speed (no direction) and significant wave height (SWH). Five altimeters which have various instrumental configurations are considered in this study: ERS; Topex/Poseidon; Jason; GFO; and Envisat. The use of remotely sensed wind and SWH in the future should potentially lead to more refined wind stress field analysis at global and regional scales.

2.3.1. ALTIMETER SWH VALIDATION

Although altimeter SWH is calibrated and validated during dedicated commissioning phase operations, after-launch long-term monitoring of the quality of the estimated geophysical parameters is needed (Queffeulou, 2003). Biases and trends are commonly observed on altimeter SWH measurements. For instance, biases of about 50 cm between TOPEX and ERS-1 and -20 cm between TOPEX and GEOSAT Follow-On (GFO) have been observed. A trend example is the TOPEX side-A SWH trend of about 40 cm between 1996 and beginning of 1999, which has been attributed to drift in the electronics. Biases are also observed on the two recent altimeters on board Jason and ENVISAT (Queffeulou, 2004).

To correct for biases and trends, methods have been developed using buoy and cross altimeter data comparisons. The buoy data from the US NDBC, the Canadian MEDS, and the European networks were used in these comparisons. Details are given in (Queffeulou, 2003 and 2004). Table 1, from (Queffeulou, 2004), gives proposed corrections to be applied to the altimeter SWH data. These corrections were established for the following altimeter data: ERS-2 Ocean PRoduct level 2 (OPR-2), TOPEX-Poseidon Merged Geophysical Data Record (M-GDR), GFO Intermediate Geophysical Data Record (IGDR), Jason Geophysical Data Record (GDR) and ENVISAT RA-2 Intermediate Marine Abridged Record (IMAR).

Correcting the data greatly reduces the differences between the various satellite data sets. There are still some differences between SWH, at global scale, but these are reduced to about 10 cm, and might be attributed to the variability resulting from the different geographical samples of the various altimeters

Note that SWH altimeter validations and corrections are regularly updated. Recent results can be found in Queffeulou and Croizé-Fillon 2010.

2.3.2. VALIDATION OVER THE WESTERN MEDITERRANEAN SEA

The validations given in section 2.3.1 were performed for the global ocean, using available buoy measurements. It could be reasonably suggested that regional validations are needed in order to take into account particular characteristics such as short fetch area, high wind variability and swell predominance.

A study (Queffeulou *et al.*, 2004) illustrates the particular SWH variability over the Western Mediterranean Sea. The TOPEX SWH measurements were compared to the data from four buoys. One of the buoys is in the Atlantic Ocean, west of Brittany ("Brittany", 47.5°N 8.5°W); the three other buoys are located in the Western Mediterranean Sea: in the Gulf of Lion ("Lion", 42.1°N 4.7°E), between the Italian coast and Corsica ("Corsica", 43.4°N 7.8°E), and south of the Balearic Islands ("Mahon", 39.72°N 4.44°E), respectively.

The TOPEX Brittany SWH comparison shows general good agreement and low scatter. Data off the Gulf of Lion are also in good agreement, though the number of data points is only 22, over a SWH range limited to 4 m. The Corsica results show an underestimate of TOPEX SWH values above 1.5 m, and larger altimeter variability than in previous cases. The interpretation is not obvious: in this area the variability of wind speed and direction is high, and the buoy is located close to the coast, leading to unusual short fetch conditions, which could affect the accuracy of the altimeter algorithm. There are also only three comparison data above 2m SWH, and the accuracy of the buoy measurement could also be involved.

Analysis of the Mahon comparisons showed that the wave direction relative to the islands has to be taken into account for altimeter validation. For some directions of the wave field, the altimeter location can be modified by the presence of the island (sheltering, refraction) while at the buoy location, the wave field is less affected by the island.

The particular examples discussed above illustrate the necessity for a careful analysis of the data over such closed seas and short fetch conditions.

2.3.3. ALTIMETER WIND SPEED VALIDATION

For ERS, TOPEX and GFO, buoy wind speed comparisons were performed (Queffeulou, 2003) and linear corrections were proposed. Jason and ENVISAT RA-2 wind speed were validated using collocated data with buoy and GEOSAT FO. Jason wind speed is underestimated by about 1 m/s relative to buoy data, and by 1.2 m/s, relative to GFO. ENVISAT wind speed is also underestimated relative to both buoy and GFO measurements by about 0.7 m/s and 0.8 m/s, respectively.

The relation between Jason and GFO wind speed is non-linear. The wind speed algorithms used are different: GFO uses the classical modified Chelton and Wentz algorithm based on σ^0 wind speed dependence, while the Jason algorithm was developed from TOPEX and QuikScat data using both SWH and σ^0 as input. This last algorithm have been tuned to Jason data (Zieger *et al.*, 2009). As for SWH, altimeter wind speed validations and data corrections are regularly updated (Queffeulou *and* Croize-Fillon, 2010)

3. OCEAN FORCING FUNCTION

3.1. Remotely sensed flux analysis

Oceanographers are particularly interested in turbulent fluxes available at regular space and time intervals (i.e. gridded fields). The objective analysis of satellite wind and latent heat flux observations is based on the kriging method described by Bentamy *et al.*. (1996). The method is applied to surface winds and latent heat flux fields separately. The aim is to calculate global daily, weekly, and monthly averaged flux parameters on a spatial grid of 0.5°×0.5° or 1°×1° (latitude×longitude) resolution. The interpolation scheme uses a spatial and temporal structure function describing the behavior of the variables. The algorithm provided by Bentamy *et al.*. (2002) is used to calculate gridded wind fields. The structure function for latent heat flux is determined using spatial and temporal correlation scales calculated from satellite observations that are about 1510 km and 65 h, respectively. These parameters are then used to evaluate the weights of the satellite observations required to estimate the weekly value, depending on their spatial and temporal position relative to the grid point under analysis. As can be expected, the number of these observations is a function of latitude. On average, more than 336 observations are used at a grid point. The lowest numbers are found in the western part of the tropical Pacific Ocean (about 120 observations). The numbers of day and night observations are about the same.

Figure 7 shows examples of weekly latent heat flux and wind speed fields over the tropical Atlantic Ocean. During the period 4 – 24 November 1996, the trade winds in both the North and South Atlantic reach mean weekly-averaged speeds of 8-10 m/s with the associated latent heat fluxes at about 200 W/m^2. Consistently higher in the northeasterly trade wind region than in the southeast trades, all three weeks illustrate the coherence between the wind and latent heat flux patterns.

3.2. Accuracy of Surface Wind analysis

The investigation of the accuracy of gridded surface parameters estimated from satellite data is only illustrated with the accuracy results related to surface wind fields. As for satellite observations, the accuracy of the gridded satellite flux analysis is determined through comparisons with buoy and numerical atmospheric estimates. For instance the comparisons between buoy and scatterometer averaged winds use the following standard statistical data analysis: The wind speed, zonal wind component, and meridional wind component are assumed to be random variables which could be characterized by their moments. For this purpose, the two conventional moments of each variable are estimated.

Moreover, some statistical parameters are calculated to assess the comparisons between satellite gridded wind fields and buoy averaged winds.

3.2.1. Global comparisons

Tables 2, 3, and 4 provide summary statistics of wind speed comparisons. The wind speed correlation coefficients are significantly high and range from 0.85 to 0.89. The rms values of the buoy-satellite differences do not exceed 1.16 m/s over the NDBC and TAO networks, but are higher for ODAS comparisons: 1.48 m/s for NSCAT, and 1.66 m/s for ERS-2. This is mainly due to a smaller number of comparison data points and to high wind variability in the ODAS area. Furthermore, the statistics calculated by several meteorological centers (ECMWF, CMM, UKMet) indicate that ODAS buoy wind speeds tend to be underestimated according to meteorological wind analysis (see ftp://ftp.shom.fr/meteo/qc-stats, site maintained by P. Blouch). The statistical parameters are also calculated in bins of 5 m/s of the buoy wind speed. Their values show small dependence on the NDBC and TAO wind speed. The bias is slightly positive for ERS and negative for NSCAT in all the wind speed ranges. The analysis carried out on collocated data, shows that the slopes calculated over each buoy network and against buoy wind estimates, are similar regardless of which of the three scatterometer wind products is used for comparison. For NDBC (Table 2), buoys and scatterometers correlate closely, as expressed by slopes (*b* and *bs*) of about 1 and intercepts of about zero. For TAO in the tropical Pacific Ocean, slopes are about 0.90, suggesting an overestimation of low wind speed and an underestimation of high wind speed by scatterometer wind fields compared to TAO winds. In the North Atlantic area, the slopes of the scatter plots are close to 1, whereas the intercepts are about 0.5, indicating that the scatterometer wind fields are consistently high compared to ODAS weekly averaged wind speeds. The calculation of statistical parameters for the ODAS buoy wind speed ranges shows that their values are made variable by the outlying points at low and high wind speeds.

No systematic wind direction bias is found, and the overall bias and standard deviation in terms of the mean angular difference are less than 8° and 38°, respectively. These results are consistent with the calibration/validation of scatterometers against buoys (Graber *et al.*, 1996 and 1997; Caruso *et al.*, 1999). For instance, in the Pacific tropical area, where the wind direction is quite steady, the standard deviation of wind direction calculated for buoy wind speed higher than 5 m/s does not exceed 17°.

3.2.2. Time series

The agreement between averaged wind fields from scatterometers and buoys can be studied using time series. Figure 8 shows examples of weekly averaged time series of wind speed at three buoy locations in the NDBC and TAO arrays, respectively. They indicate that the matchups are strongly correlated, and their geographical features compare well. The lowest correlation values (less than 0.91) are found in the TAO array. At the 95°W-2°N TAO (Figure 8c), the difference is consistent and the bias is about 1m/s. This may be related to the south equatorial current effect on scatterometer backscatter coefficient measurements (Quilfen *et al.*, 2001). Indeed, the buoy samples the absolute wind, whereas the scatterometer samples the relative wind. The highest discrepancy between TAO and scatterometer winds (bias greater than 1.5 m/s) occurred between May and December 1998. During this period, several scatterometer retrieval winds are not valid (especially during May and June 1998), and the TAO buoy moored at this location reported high variable winds of about 7 m/s, exceeding climatology by 1 m/s. The standard deviation of weekly averaged buoy wind speed varies between 0.9 m/s and 1.9 m/s (72% of standard deviation values are great than 1.2 m/s). Furthermore, the analysis of oceanic current measured at 110°W, 2°N indicate that its magnitude is about 50 cm/s from May through December 1998, while for 1992 until 1997 and during the same months, the current magnitude is on average 30 cm/s. The comparisons between NDBC and scatterometer averaged wind speed time series do not exhibit any systematic bias (an example is shown in Figure 8a). At some locations a seasonal variation in the differences is found. The bias tends to be positive in winter and negative in summer. This may be related to the dependence of wind speed residuals on buoy wind speed ranges illustrated by the results of Table 2. For ODAS (not shown), scatterometer averaged wind speeds are consistently higher than buoy estimates. However, the bias tends to be large between October and December 1996, when the correlation coefficient is about 0.69. The latter is lower than for the whole period. by a factor of 22%.Some discrepancies between buoys and scatterometers are related to the sampling errors of scatterometer wind fields. For instance, between July and August 1996, the ERS-2 error exceeds 2 m/s due to the relatively small number of scatterometer observations available to estimate the gridded fields.

Finally, the dependence of the residuals on the buoy latitude is investigated. More than 80% of the latitudinal differences are less than 0.5 m/s. Between 8°S and 2°N latitudes (TAO array), the bias (buoy minus scatterometer) is positive and continuous with increasing latitude. This dependency is consistent with results shown above and might be due to current and sea state. From 5°N to 45°N, a slightly decreasing bias is exhibited. At high latitudes, where the wind is highly variable, scatterometer weekly wind speeds tend to be overestimated against buoy estimates. This is mainly related to the methods used to average wind data from scatterometers and buoys, and to the sampling scheme. The analysis of the rms behavior with latitude confirms the latter results. Indeed, most of the values of the rms difference between buoys and scatterometers are below 1.2 m/s, except at latitudes above 45°N.

To examine the agreement between weekly averaged scatterometer and buoy winds as a function of buoy latitude, the correlation coefficient for each latitude is calculated. The main results of these statistical parameters are higher than 0.8 for all latitudes and the differences between them are not significant at the 95% confidence level.

3.2.3. Scatterometer / ECMWF averaged wind comparisons

In this section, the new mean weekly and monthly scatterometer wind fields are compared to the ECMWF operational surface wind analyses. Like several National Weather Prediction (NWP) systems, ECMWF is a very complex analysis system which is continually being improved. It assimilates measurements from a variety of sources: satellites, buoys, and ships. It is important to notice that ECMWF products are not used as a "ground truth" for surface winds. However, they represent the main known wind features at various scales and in all oceanic basins. Their use allows the investigation of scatterometer wind field patterns over a given ocean basin and/or time period. Furthermore, as the scatterometer data are uniformly processed, they can be used to evaluate the impact of the numerous changes that have occurred in the ECMWF forecast-analysis system. The mean weekly and monthly ECMWF wind speed, zonal component and meridional component are computed from the 6-hourly global analysis datasets on 1°.125×1°.125 grid. The scatterometer sea ice mask is used to avoid ice.

The comparisons are performed over the global ocean for all December and June months of the ERS-1, ERS-2 and NSCAT periods. Only ECMWF wind speeds above 3 m/s and estimated over oceanic regions are used. Statistics of the comparisons are summarized in Table 5. The correlations for wind speed, zonal wind component, meridional wind component, and wind direction are high and exceed 0.89. For wind direction, the biases are small, while the rms values are 28° for ERS-1, 26° for ERS-2, and 17° for NSCAT. Even if the wind speed biases are rather low, ERS-1 and NSCAT are biased high by about 0.50 m/s compared to ECMWF, while the corresponding rms values are 1.40 m/s for ERS-1 and 1.03 m/s for NSCAT. The number of high wind condition events derived from ERS-1 and NSCAT is high with respect to ECMWF. More than 6.5% of ERS-1 and NSCAT wind speed estimates exceed 15 m/s and this percentage drops to 4.5% for ECMWF. Comparisons between ECMWF and ERS-2 provide the lowest bias and rms values of 0.04 m/s and 0.96 m/s, respectively. Most of significant discrepancies between ECMWF and scatterometers are located at high latitudes in both hemispheres poleward of 60°. However, in some cases of low correlations are found in middle latitudes. For instance, the correlation coefficient, calculated in the South Atlantic region between 35°S and 45°S for the period 7 - 13 December 1992 is 0.42. For this week and region, the kriging error measuring the quality of weekly averaged winds does not exceed 1m/s. The annual mean profiles, estimated as longititudinal averages of the scatterometer and ECMWF winds in 1° latitude bands, indicate that scatterometer and ECMWF wind features compare well. The highest wind values are found in the 50°S – 60°S and 50°N – 60°N bands. Lowest winds occur within equatorial regions. For instance, at 53°S, scatterometer and ECMWF provide wind speed averages of about 9.5 m/s, while at 0° the annual mean wind speed is about 5 m/s. The highest differences exceeding 0.5 m/s are found in the 55°N – 65°N belt. However, such a calculation indicates that scatterometer wind speeds are greater than ECMWF estimates almost everywhere. Figure 9 displays examples of latitudinal weekly scatterometer and ECMWF wind speed comparisons. The time series are calculated from 1°×1° gridded fields integrated over three 20° latitude bands over the Atlantic Ocean. They show that the correlation is high and roughly constant over the whole period. Scatterometer and ECMWF winds exhibit similar wind features. In particular, the examples do not show any disturbing oscillations in scatterometer winds. Furthermore, such calculations confirm that the ERS-1 scatterometer records higher winds than ECMWF. The maximum differences between ERS-1 and ECMWF winds occurred between 9 December 1991 and 24 February 1992, corresponding to many missing data in scatterometer observations due to the ERS-1 scatterometer calibration/validation process. However, the calculation of the relative differences $((W_{ecmwf} - W_{scat})/(W_{ecmwf}+W_{scat})/2)$ indicate that on average their values in equatorial regions decrease from 12% to 2% between March 1992 and September 1994, while in high latitudes these values are nearly steady and are about 5%. For ERS-2, the differences between ECMWF and scatterometer winds are the lowest. ERS-2 scatterometer measurements have been assimilated within the ECMWF analysis scheme since April 1996. Except in the Atlantic sector of the Southern Ocean, average weekly winds estimated from NSCAT observations, are higher than ECMWF wind estimates. The variability of the difference between ECMWF and scatterometer weekly wind fields is investigated in terms of rms differences (Figures not shown). Excluding periods when there are many missing scatterometer data, the average rms difference in wind speed is less than 1.5 m/s in the middle and tropical latitudes. In high latitudes and due to high wind variability, the rms difference values are high and about 2 m/s. Similar geographical features are found in terms of wind components. As expected, the rms difference between ECMWF and ERS-2 is 0.5 m/s lower than the rms difference between ECMWF and ERS-1. The analysis of the rms difference patterns according to time indicates that there is a decreasing trend mainly related to ECMWF model changes (ECMWF, 1993). Furthermore, the rms features are highly correlated to seasonal wind variability. For instance, in high northern latitudes the rms differences are lower between April and September with a mean value of about 0.8 m/s for wind speed. The behavior of the rms differences between ECMWF and NSCAT weekly wind speed and components is found to be quite comparable to that estimated from ECMWF and ERS-2 differences.

4. SUMMARY

A brief review of the methods for extracting surface winds from scatterometers, altimeters, and radiometers has been given. The allowance for wind conditions, sea state, and atmospheric effects has been discussed and empirical corrections have been outlined. The surface wind retrievals are used to enhance the determination of turbulent flux components such as wind stress and latent heat flux. In this study, only scatterometer and SSM/I winds in combination with the specific air humidity retrieved from the radiometer brightness temperatures are used for estimating surface fluxes. They allow the determination of accurate weekly and monthly turbulent flux field over global ocean. In future studies, retrievals from altimeters and from ASCAT scatterometer will also be considered to improve the spatial and temporal resolutions as well the quality of the forcing function components.

Weekly and monthly flux data including, wind speed, zonal and meridional components, wind stress and the associated components, latent and sensible heat fluxes, are freely available at the following addresses:

- ERS-1/2 L2b winds:
  http://cersat.ifremer.fr/fr/data/discovery/by_parameter/ocean_wind/ers_wnf
- ERS-1/2 L4b wind products:
  http://cersat.ifremer.fr/fr/data/discovery/by_parameter/ocean_wind

- NSCAT and QuikSCAT L2b wind products
  http://podaac.jpl.nasa.gov/DATA_PRODUCT/OVW
- NSCAT L4b wind products:
  http://cersat.ifremer.fr/fr/data/discovery/by_parameter/ocean_wind/mwf_nscat
- QuikSCAT L4b wind products:
  http://cersat.ifremer.fr/fr/data/discovery/by_parameter/ocean_wind/mwf_quikscat
- Satellite turbulent fluxes:

ftp://ftp.ifremer.fr/ifremer/cersat/products/gridded/flux-merged/flux/data/

References

Ataktürk, S. S., and K. B. Katsaros, 1998: Estimates of surface humidity and wind speed obtained from satellite data in the stratocumulus regime in the Azores region. *Remote Sensing of the Pacific Ocean by Satellites,* R. A. Brown, Ed., Southwood Press, 16-22.

Bentamy, A., Y. Quilfen, P. Quefeulou, and A. Cavanié, 1994: Calibration and validation of the ERS-1 scatterometer. IFREMER Tech. Rep. DRO/OS-94-01, 80 pp.

Bentamy, A., Y. Quilfen, F. Gohin, N. Grima, M. Lenaour, and J. Servain, 1996: Determination and validation of average field from ERS-1 scatterometer measurements. *Global Atmos. Ocean Sys.*, **4**, 1-29.

Bentamy A, P. Queffeulou, Y. Quilfen and K. Katsaros, 1999 : Ocean surface wind fields estimated from satellite active and passive microwave instruments, *IEEE Trans. Geos. Rem. Sens*., Vol 37, No 5, 2469-2486.

Bentamy, A, Y. Quilfen and P. Flament, 2002 : Scatteromter wind fields : a new release over the decade 1991-2001.*CJRS*, Vol 28, No 3, 424-430.

Boutin, J., J. Etcheto, M. Rafizadeh and D. C. E. Bakker, 1999 : Comparison of NSCAT, ERS-2 active microwave instrument, special sensor microwave imager, and carbon interface ocean atmosphere buoy wind speed : consequences for the air-sea CO2 exchange coefficient, J. Geophys. Res., 104, 11375-11392.

Ebutchi, N, 1999 : Statistical distribution of wind speeds and directions globally observed by NSCAT, J. Geophys. Res., 103, 7787-7798.

Freilich, M. H. and S. Dunbar, 1999 : The accuracy of the NSCAT 1 vector winds : Comparisons with National Data Buoy Center buoys, *J. Geophys. Res*., 104, 11231-11246

Goodberlet, M. A., C. T. Swift, and J. C. Wilkerson, 1989: Remote sensing of ocean surface winds with the Special Sensor Microwave/Imager. *J. Geophys. Res.,* **94**, 14,547-14,555.

Graber H. C., N. Ebutchi, R. Vakkayil, 1996 : Evaluation of ERS-1 scatterometer winds with wind and wave ocean buoy observations, Tech. Report, RSMAS 96-003, Division of Applied Marine Physics, RSMAS, Univ. of Miami, Florida 33149-1098, USA, 58 pp..

Grima, N., A. Bentamy, K. Katsaros, and Y. Quilfen, 1999: Sensitivity of an oceanic general circulation model forced by satellite wind stress fields. *J. Geophys. Res.*, **104**, 7967-7989.

Hosking, J. R. M., 1990: L-moments : analysis and estimation od distributions using linear combinations of order statistics, *J. R. Statist, Soc. Ser*. B, **52**, 105-124.

Jones, W. L., F. J. Wentz and L. Schroeder, 1978 : Algorithm for inferring wind stress from Seasat-A, *J. Spacecraft and Rockets*, 15, 368-374

Katsaros, K.B., A.M. Mestas-Nuñez, A. Bentamy, E.B. Forde, 2003: Wind bursts and enhanced evaporation in th tropical and subtropical Atlantic Ocean. In Interhemispheric Water Exchange in the Atlantic Ocean, G. Goni and P. Malanotte- Rizzoli (eds.). Elsevier Oceanographic Series.463 – 474.

Liu W. T., K. Katsaros, and J. A. Businger, 1979 : Bulk parametrization of air-sea exchanges of heat and water vapor including the molecular constraints at the interface, *J. Atmos. Sci*., Vol 36, 1722-1735.

Liu, W. T., 1986: Statistical relation between monthly precipitable water and surface-level humidity over global oceans. *Mon. Wea. Rev.*, **114**, 1591-1602.

Liu W., T. W. Tang and P. S. Polito, 1998 : NASA scatterometer provides global ocean-surface wind fields with more structures than numerical weather prediction. *Geophys. Res. Lett*., 25, 761-764.

Miller, D. K. and K. . Katsaros, 1992 : Satellite derived surface latent heat fluxes in rapidly intensifying mariner cyclone, *Mon. Wea. Rev*., 120, 1093-1107

Millif, R. F., W. G. Large, J. Morzel, G. Danabasoglu and T. M. Chin, 1999 : Ocean genertal circulation model sensitivity to forcing from scatterometer winds, *J. Geophys. Res*., 104, 11337-11358.

Millif, R. F., M. h. Freilich, W. T. Liu, R. Atlas and W. G. Large, 2001 : Global ocean surface wind observations from space. *Proc. Internation. Conf. Ocean. Observations for Climate Chnages*, CSIRO Press.

Pegion, P. J., M. A. Bourassa, D. M. Legler, and J. J. O'Brien, 2000: Objectively derived daily "wind" from satellite scatterometer data. Month. Weat. Rev, Vol 128, 3150-3168.

Queffeulou P., 2003: Cross-validation of ENVISAT RA-2 significant wave height, sigma0, and wind speed. IFREMER Final report, May 2003..

Queffeulou P., A. Bentamy and J. Guyader, 2004: Satellite wave height validation over the Mediterranean Sea, Proceedings of the ENVISAT & ERS symposium, Salzburg, Austria, 6-10 September 2004.

Queffeulou P., 2004: Long-term validation of wave height measurements from altimeters. Marine Geodesy, 27, pp 495-510.

Queffeulou P. et D. Croizé-Fillon, Global altimeter SWH data set, version 7, May 2010, ftp://ftp.ifremer.fr/ifremer/cersat/products/swath/altimeters/waves/

Quilfen, Y., 1995: ERS-1 off-line wind scatterometer products. IFREMER Tech. Rep., 75 pp.

Quilfen, Y, , Chapron, B., Vandemark, D., 2001, "The ERS Scatterometer Wind Measurement Accuracy: Evidence of Seasonal and Regional Biases", J. Atmospheric and Oceanic Technology, vol. 18, no. 10, pp. 1684-1697.

Schlüssel, P., L. Schanz, and G. English, 1995: Retrieval of latent heat flux and long wave irradiance at the sea surface from SSM/I and AVHRR measurements. *Adv. Space Res.*, **16**, 107-115.

Schulz, J., P. Schlüssel, and H. Grassl, 1993: Water vapor in the atmospheric boundary layer over oceans from SSM/I measurements. *Int. J. Remote Sens.,* **14**, 2773-2789.

Shultz, J, , J. Meywerk, S. Ewald, and P. Schlüssel, 1997: Evaluation of satellite-derived latent heat fluxes. *J. Climate,* **10**, 2782-2795.

Sobieski P., C. Craeye, and L. Bliven, 1999 : Scatterometric signatures of multivariate drop impacts on fresh and salt water surfaces,' *Intl Jl of Remote Sensing*, Vol. 20, n° 11, July 1999, pp. 2149-2166.

Stoffelen, A. and D. Anderson, 1997 : Scatterometer data interpretation : Estimation and validation of the transfer function CMOD4, *J. Geophys. Res*., 102, 5767-5780.

Thiria, S., C. Mejia, F. Badran and M. Crepon, 1993 : A neural network approach for modeling nonlinear transfer functions : Application for wind retrieval from spaceborne scatterometer data, *J. Geophys. Res*., 98, 22827-22841.

Zieger S, Vinoth J,Young IR, 2009: Joint Calibration of Multiplatform Altimeter Measurements of Wind Speed and Wave Height over the Past 20 Years. Journal of Atmospheric and Oceanic Technology 26(12)

Wentz, F. J. and D. K. Smith, 1999: A model function for the ocean-normalized radar cross-section at 14GHz derived from NSCAT observations, *J. Geophys. Res*., 104, 11449-11514

Tables

Table 1 Summary of the proposed linear corrections to altimeter SWH measurements (SWH_cor = a * SWH + b). n=number of comparison data points

Satellite	reference	n	a	b
ERS-2	Buoys	12070	1.0642	0.0006
TOPEX-A [(1)]	Buoys	2562	1.0539	-0.0766
TOPEX-B	Buoys	7826	1.0237	-0.0476
Poseidon	Buoys	752	0.9914	-0.0103
GFO	TOPEX	15974	1.0625	0.0754
Jason	GFO	6332	1.0587	-0.0571
ENVISAT	GFO	1428	1.0526	-0.1991

[(1)] TOPEX side-A has to be further corrected as a function of cycle number, for cycle 98 to 235:
$swh_{cor} = swh + poly3(98) - poly3(cycle)$ with $poly3(x) = \sum a_i \times x^i$
and $a_0 = 0.0864$; $a_1 = -6.0426 \times 10^{-4}$; $a_2 = -7.7894 \times 10^{-6}$; $a_3 = 6.9624 \times 10^{-8}$

Table 2: Comparison of averaged weekly wind speed and direction estimated from NDBC buoy measurements and from ERS-1, ERS-2 and NSCAT scatterometer observations. Bias, root mean square (Rms), correlation coefficient (ρ) and the standard deviation characterizing the difference between buoy and scatterometer averaged wind speeds and directions are provided.

Data SET	BuoyWind Speed Range (m/s)	Length	Wind Speed (m/s)			Wind Direction	
			Bias (m/s)	Rms (m/s)	ρ	Bias (deg)	Std (deg)
NDBC / ERS-1	0-24	3281	0.02	1.16	0.86	3	35
	0-5	320	-0.14	1.03	0.74	5	47
	5-10	2603	0.05	1.16	0.83	3	34
	> 10	358	-0.0	1.31	0.76	3	30
NDBC / ERS-2	0-24	1921	0.35	1.15	0.86	6	33
	0-5	142	0.06	0.82	0.75	0	47
	5-10	1581	0.37	1.16	0.83	6	33
	> 10	198	0.40	1.26	0.77	6	25
NDBC / NSCAT	0-24	522	-0.37	1.02	0.88	8	25
	0-5	28	-0.54	0.94	0.76	3	29
	5-10	444	-0.37	1.01	0.85	8	26
	> 10	50	-0.32	1.15	0.79	7	15

Table 3 : Comparison of averaged weekly wind speed and direction estimated from TAO buoy measurements and from ERS-1, ERS-2 and NSCAT scatterometer observations.

Data SET	BuoyWind Speed Range (m/s)	Length	Wind Speed (m/s)			Wind Direction	
			Bias (m/s)	Rms (m/s)	ρ	Bias (deg)	Std (deg)
TAO / ERS-1	0-24	10047	0.29	0.89	0.86	3	31
	0-5	3262	-0.14	0.85	0.76	1	51
	5-10	6693	0.47	0.91	0.84	5	17
	> 10	92	0.24	0.92	0.70	8	9
TAO / ERS-2	0-24	6737	0.56	1.03	0.86	3	27
	0-5	1925	0.06	0.84	0.75	4	45
	5-10	4736	0.75	1.10	0.85	5	16
	> 10	76	0.76	1.14	0.78	7	10
TAO / NSCAT	0-24	1780	-0.26	0.92	0.92	5	20
	0-5	515	-0.70	1.18	0.74	2	33
	5-10	1246	-0.08	0.79	0.83	7	11
	> 10	19	0.03	0.82	0.78	10	5

Table 4 : Comparison of averaged weekly wind speed and direction estimated from ODAS buoy measurements and from ERS-2 and NSCAT scatterometer observations

Data SET	BuoyWind Speed Range (m/s)	Length	Wind Speed (m/s)			Wind Direction	
			Bias (m/s)	Rms (m/s)	ρ	Bias (deg)	Std (deg)
ODAS / ERS-2	0-24	222	-0.73	1.69	0.84	1	38
	0-5	10	-1.26	2.01	0.72	31	75
	5-10	155	-0.61	1.68	0.80	3	39
	> 10	57	-0.83	1.50	0.80	4	22
ODAS / NSCAT	0-24	194	-0.65	1.52	0.89	2	30
	0-5	6	-1.29	2.07	0.72	14	76
	5-10	118	-0.62	1.44	0.81	1	30
	> 10	70	-0.57	1.47	0.86	9	22

Table 5 : Comparison of averaged weekly wind speed and direction estimated from ECMWF wind analysis and from ERS-1, ERS-2 and NSCAT scatterometer observations

Data SET	**Wind Speed (m/s)**			**Wind Direction**	
	Bias (m/s)	**Rms (m/s)**	ρ	**Bias (deg)**	**Std (deg)**
ECMWF / ERS-1	-0.39	1.42	0.89	1	28
ECMWF / ERS-2	0.04	0.96	0.94	0	26
ECMWF / NSCAT	-0.57	1.03	0.92	5	17

Figures

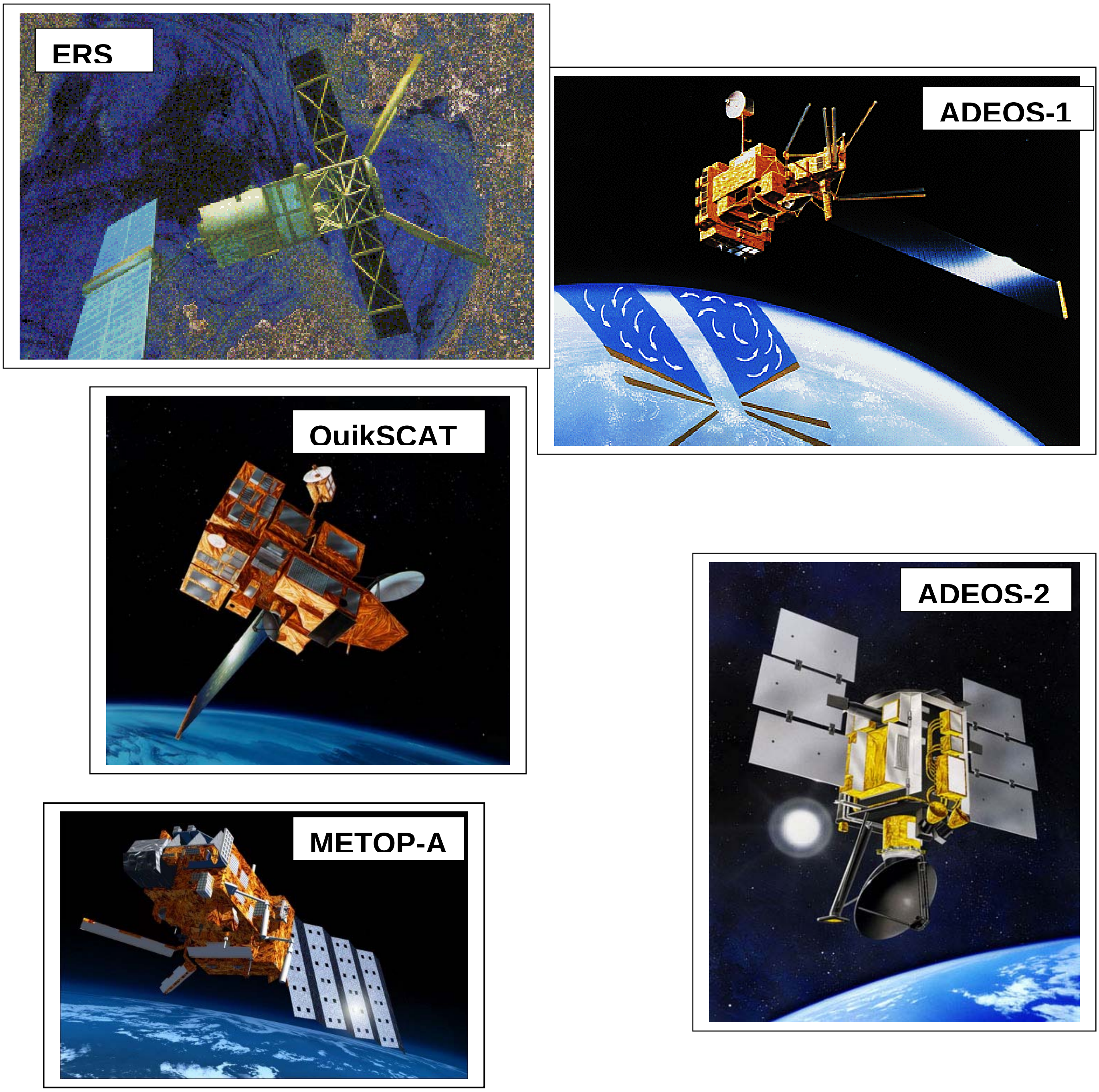

Figure 1: Satellites carrying scatterometers launched since 1991.

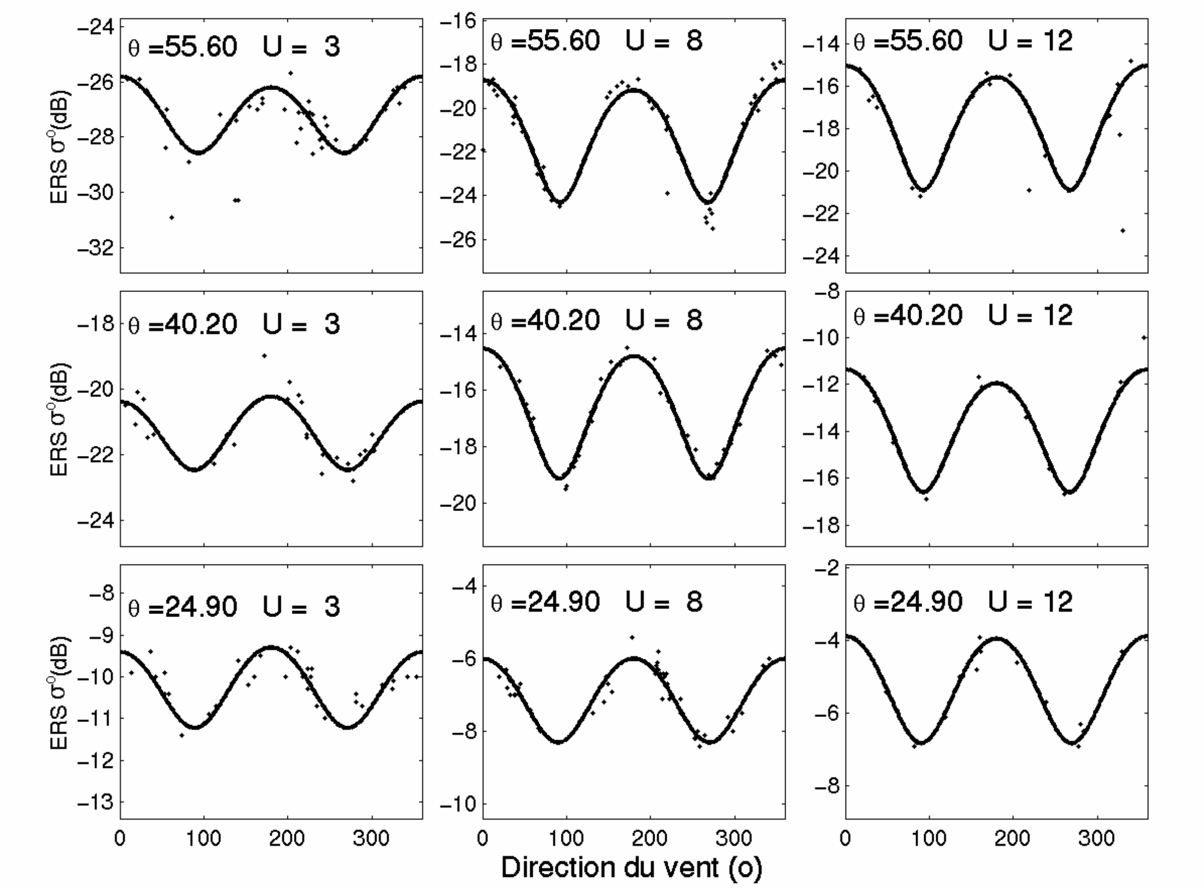

Figure 2: Behaviour of the backscatter coefficient (σ^0) measured by the ERS scatterometer as a function of relative wind direction for three wind speeds (columns) and three incidence angles ranges (rows). The solid line indicates σ^0 estimated from GMF (Eq. 1) while dots indicate the measured σ^0.

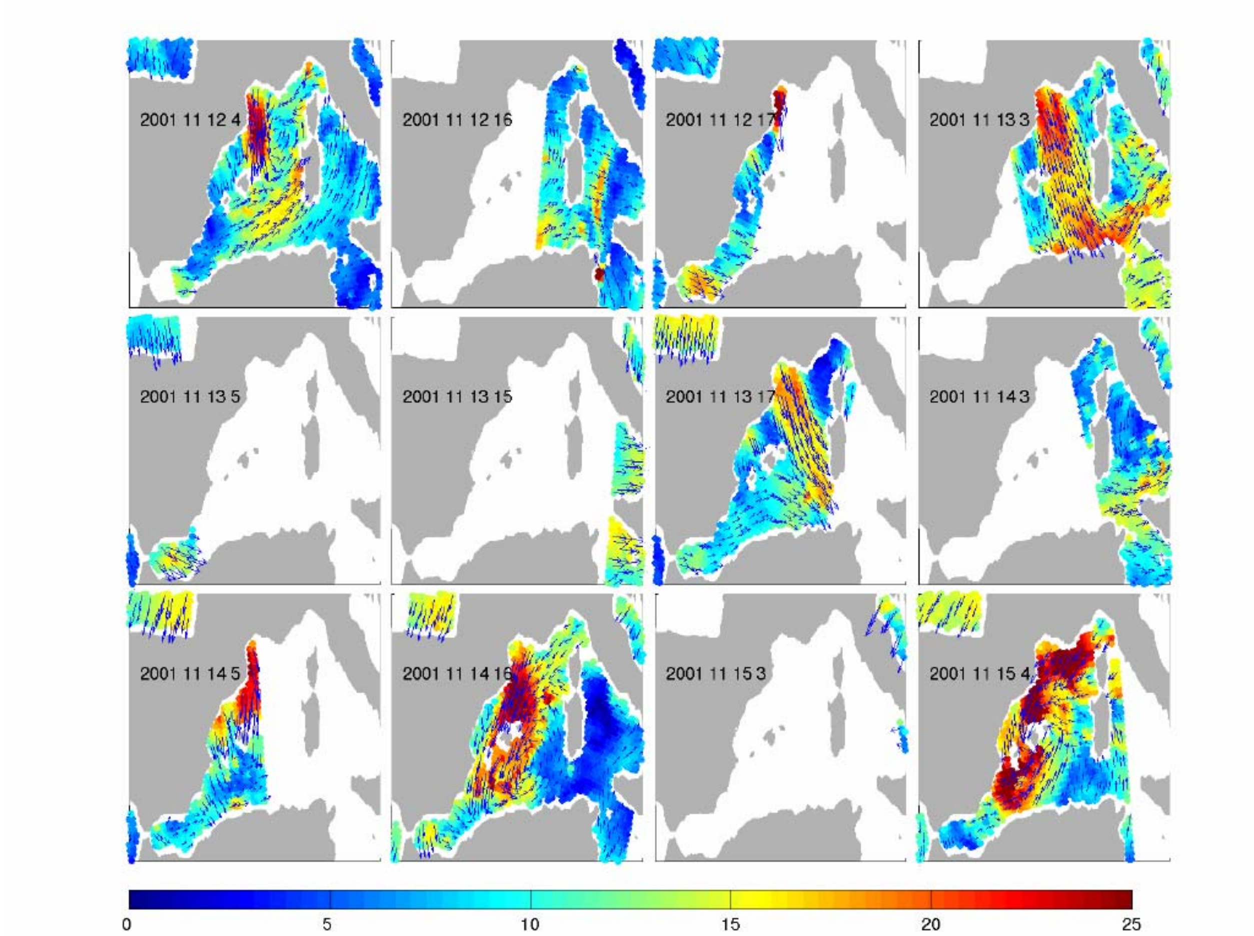

Figure 3: Example of retrieved wind speed (in colour) and direction (arrow) estimated over QuikScat swath from 12th to 15th November 2001. The approximated swath date is shown in the top left area of each panel (Year, Month, Day, Hour).

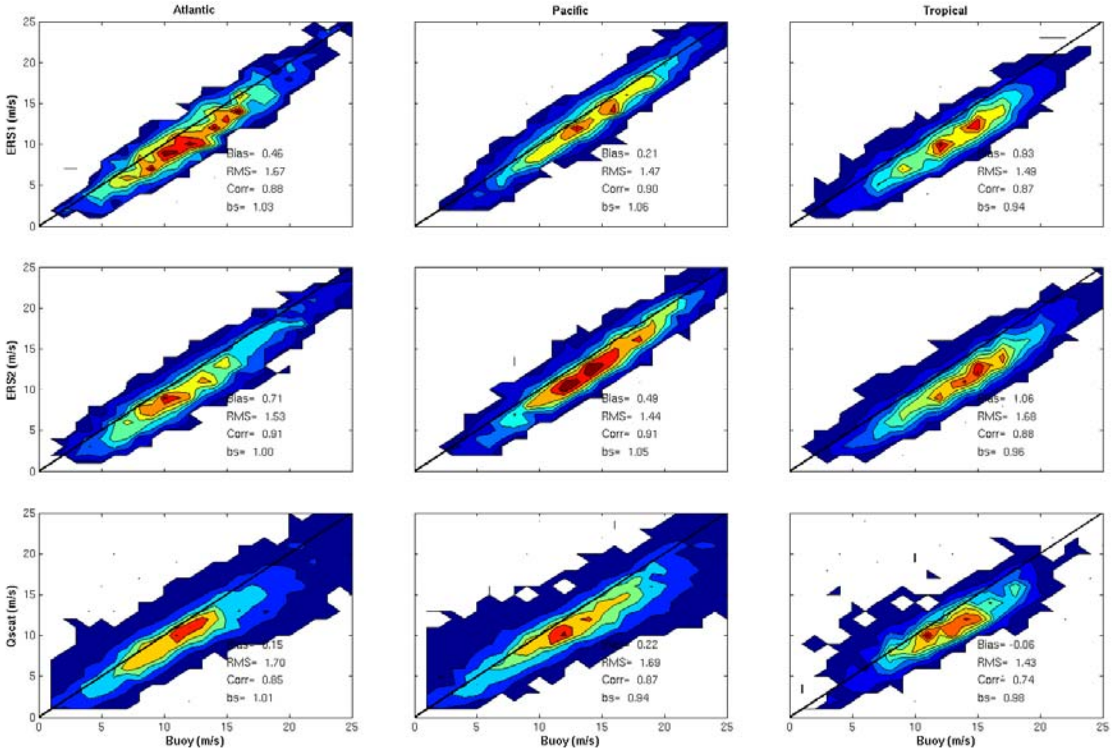

Figure 4: Comparison of the wind speeds (left panel) and directions (right panel) observed by ERS-1 (top), ERS-2 (middle), and QuikScat (bottom) scatterometers with 10-m buoy winds moored in the Atlantic Ocean (first column), the Pacific Ocean (second column), and in the Tropical oceans (third column).

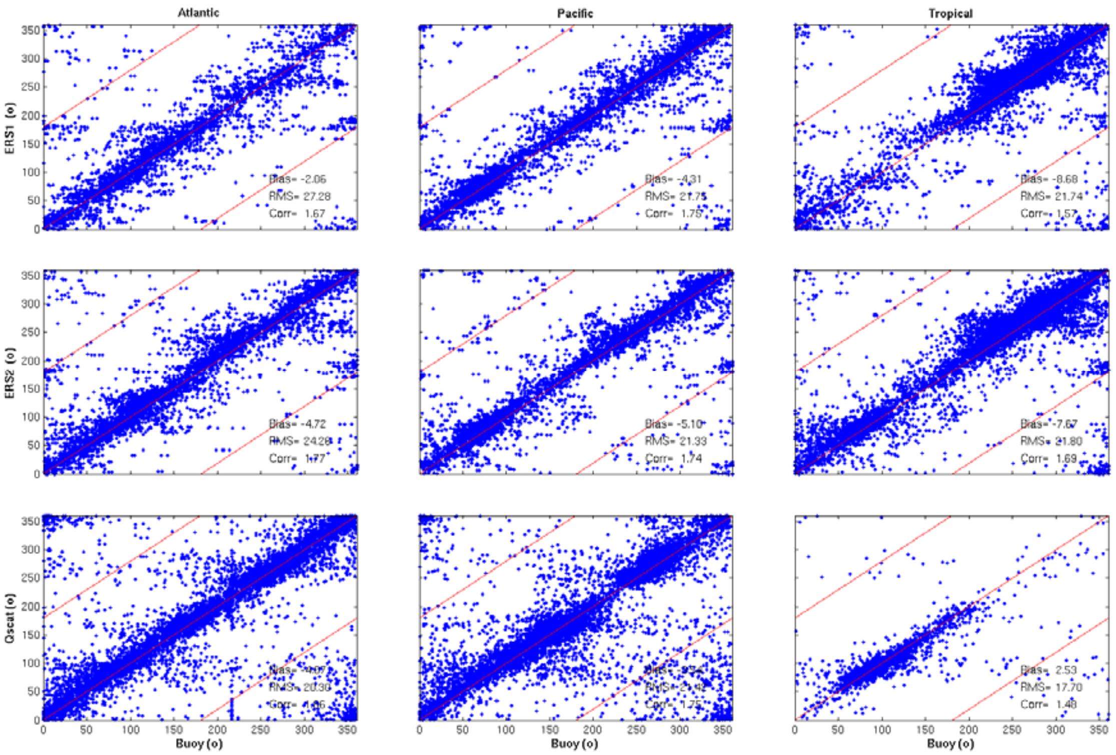

Figure 5: As Figure 4 for wind direction comparisons.

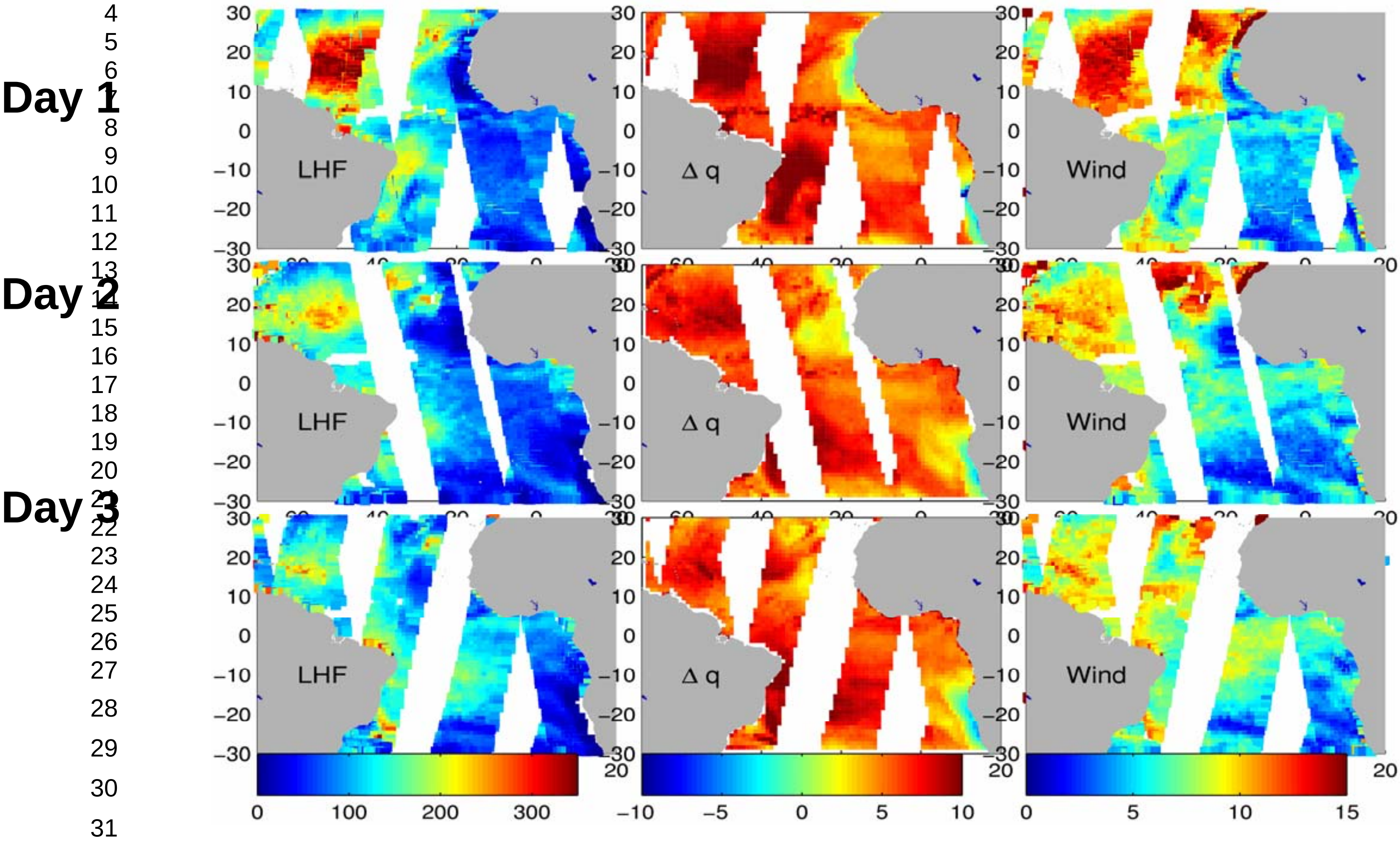

Figure 6: Three days of latent heat flux (left column), specific surface and air humidity difference (middle), and surface wind speed (right column) estimated from satellite measurements.

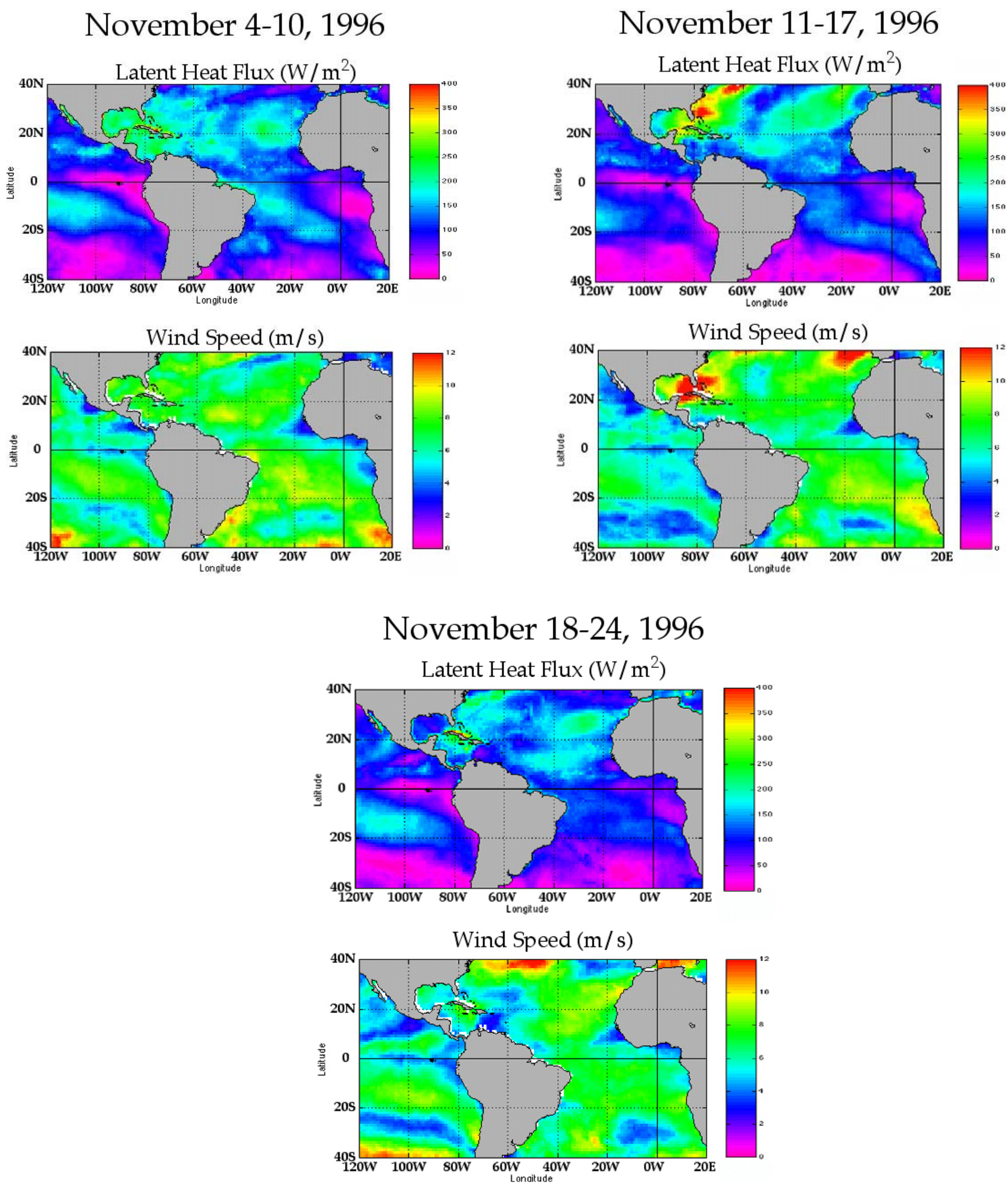

Figure 7. Sequence of three weeks in November 1996 showing pairs of weekly averaged maps of surface wind speed and latent heat flux. The week of November 11-17 (upper right) shows the effects of a high wind event blowing from the Atlantic Ocean towards the Gulf of Mexico with intensely enhanced latent heat flux (from Katsaros *et al.*, 2003).

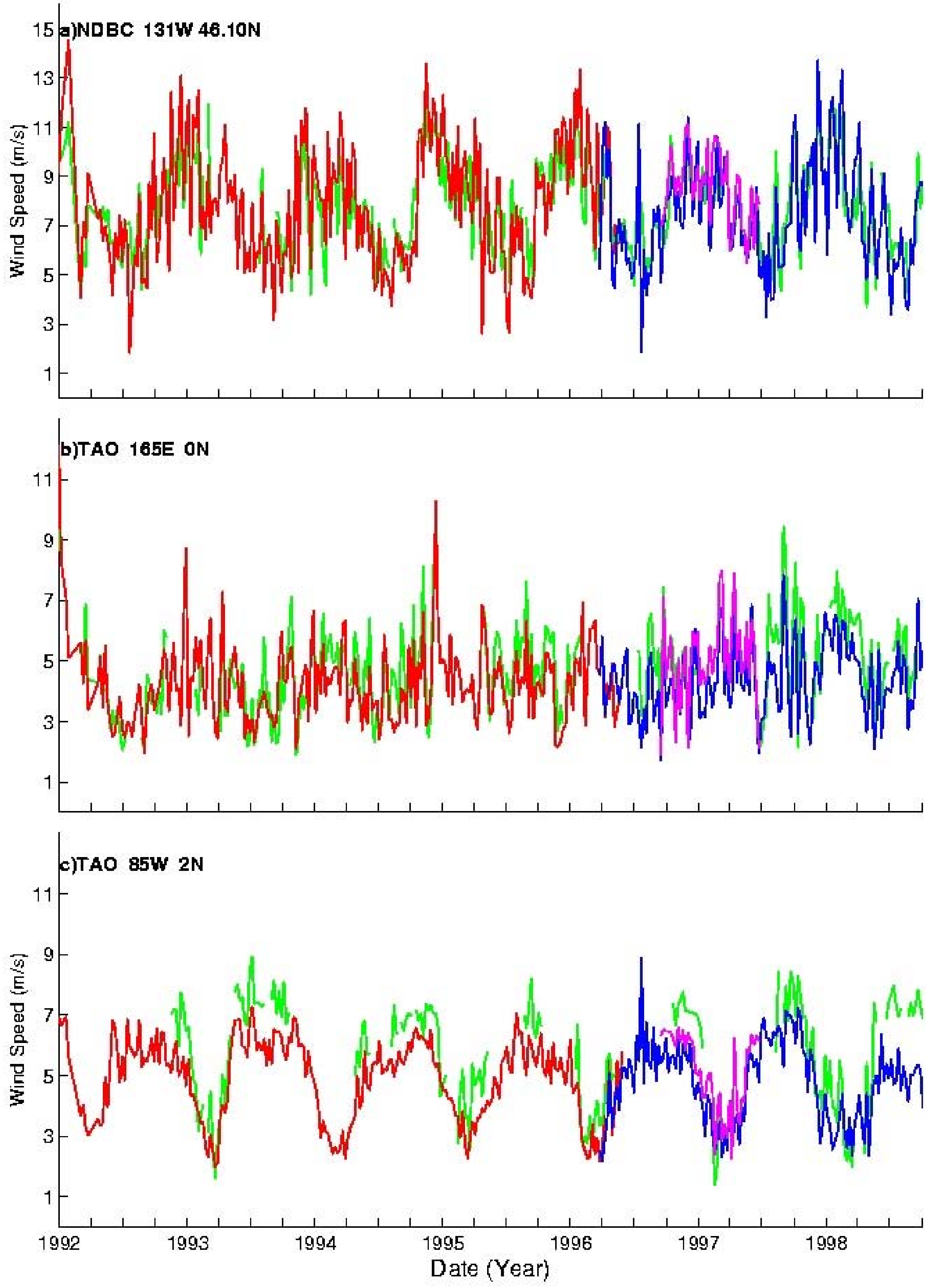

Figure 8: Time series of buoy (green), ERS-1 (red), ERS-2 (blue), NSCAT (cyan) wind speed at three buoy locations.

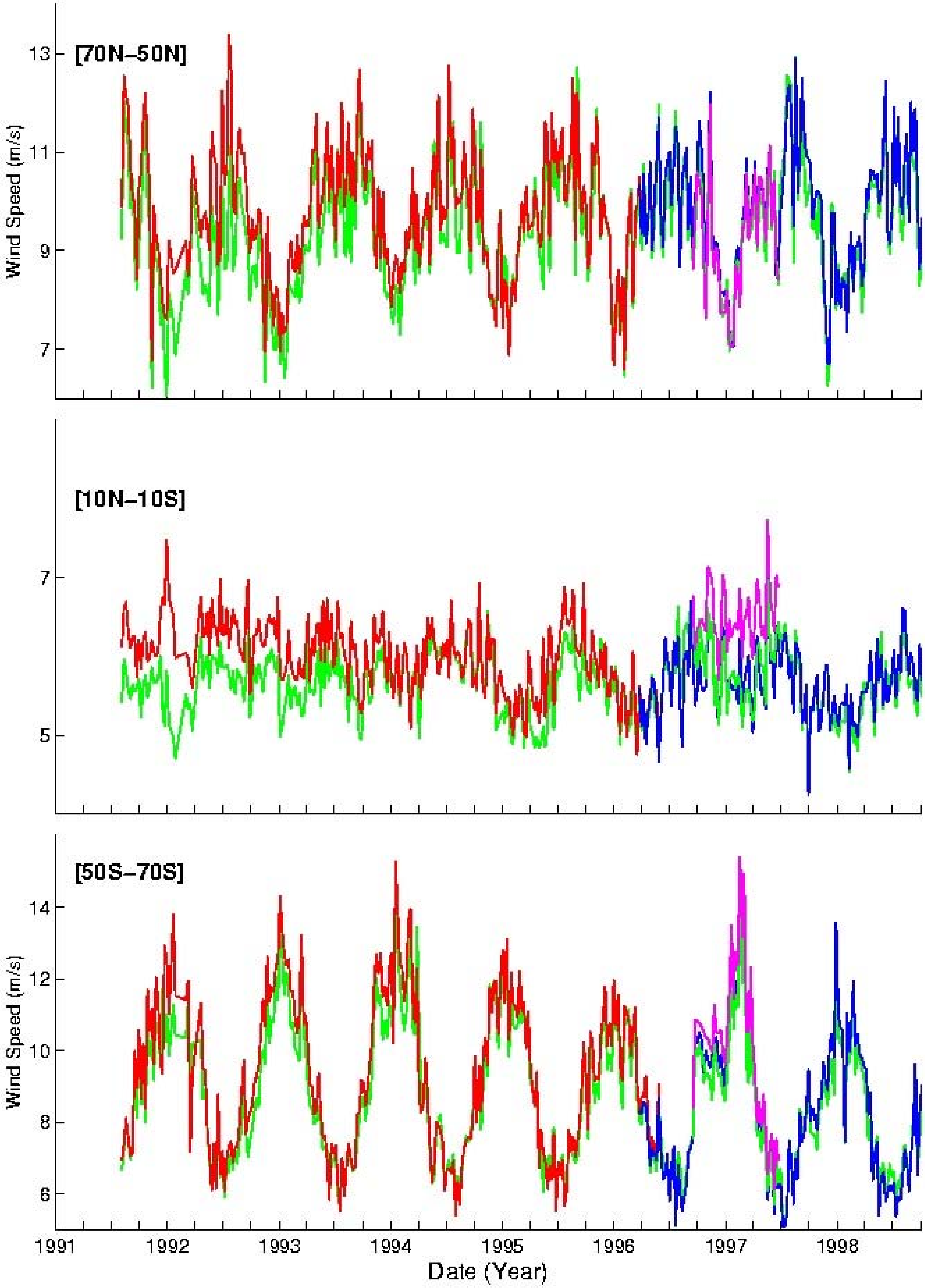

Figure 9 : Time series of averaged ECMWF (green), ERS-1 (red), ERS-2 (blue), NSCAT (cyan) wind speed estimated over three oceanic areas.